A TIME-DEPENDENT-COEFFICIENT REDUCED-ORDER MODEL FOR UNSTEADY AERODYNAMICS OF PROPROTORS

M. Gennaretti and L. Greco
University Roma Tre
Dept. of Mechanical and Industrial Engineering
via della Vasca Navale 79
00146 Rome - Italy

Abstract

This work presents a methodology for the identification of a periodic-coefficient Reduced-Order Model (ROM) for the prediction of perturbation aerodynamic loads on tiltrotor propellers in cruise flight. Although the result is a periodic-coefficient model, the process requires only frequency-domain aerodynamic solutions. Assuming the unperturbed proprotor in axial flow, first the matrix collecting the aerodynamic transfer functions between blade perturbative boundary conditions and generalized aerodynamic forces is derived. Then, its rational-matrix approximation followed by the combination with the equations describing the kynetic coupling between wing and proprotors yields the aerodynamic ROM. This ROM is expressed in terms of a set of linear equations that relate the time evolution of the aerodynamic loads acting on the proprotor blades to wing and deformable-blade degrees of freedom. Numerical results concerning a three-bladed proprotor fixed to a bending and twisting wing will show that the unsteady aerodynamic loads predicted by the proposed ROM are in excellent agreement with those obtained through direct time-marching aerodynamic solutions.

1. Introduction

The aim of the present paper is the identification of a periodic-coefficient Reduced-Order Model (ROM) for the prediction of unsteady aerodynamic loads on tiltrotor propellers (proprotors) in axial motion. In spite of the fact that it has time periodic coefficients, the proposed procedure is based only on frequency-domain aerodynamic solutions. This ROM relates perturbations to wing-proprotor motion (and gust-induced velocity, if present) to blade generalized aerodynamic forces. When combined with the structural equations, it yields a simple mathematical description of the wing-proprotor system that is suitable for multidisciplinary preliminary design purposes and, at the same time, is capable to predict the perturbed dynamic behavior with a high level of accuracy and low computational cost.

In last few years, the development of simulation tools for the aeroelastic analysis of tiltrotors has captured the attention of many researchers (see, for instance, Refs. [1], [2], [3], and [4]). This is a very complex phenomenon where a strong interaction between wing and proprotor occurs both in terms of kynetic coupling and in terms of aerodynamic interference. It follows that the use of a direct CFD simulation for the evaluation of the aerodynamic loads acting on a wing-proprotor system requires a considerable computational effort. Hence, simplified (and as accurate as possible) models are highly desirable, especially for design and control-law tailoring purposes. Nonetheless, most of the work in the field of tiltrotor aeroelasticity is focused on the development of wing-proprotor structural models (although sporadic examples of development of unsteady aerodynamic models are available in literature such as, *e.g.,* in Ref. [5]) and, typically, very simple 2D, quasi-steady models combined with the strip-theory approach, are used for the prediction of aerodynamic loadings (see, *e.g.,* Refs. [1], [2], and [4]).

The approximate aerodynamic model presented here for describing unsteady forces on proprotor blades is based on a 3D, unsteady aerodynamic solution. The motion of the proprotor is assumed

to be affected by that of the wing; however, the effect of proprotor-wing aerodynamic interference is not included in the analysis. Specifically, considering the proprotor in axial flow (*i.e.,* the case of a tiltrotor in cruise flight), our goal is the identification of a ROM describing the unsteady aerodynamic forces induced by motion perturbations due to blade flexibility and kynetic coupling with the wing. This model consists of a set of linear equations that relate the time evolution of the aerodynamic loads acting on the proprotor blades to the perturbations of wing and deformable-blade degrees of freedom (along with their first and second time derivatives). Due to the kynetic coupling between these perturbations and rotary motion of the blades, the equations have periodic coefficients. In addition, the inclusion of the flow memory effects produced by the proprotor wake vorticity yields the introduction of a finite number of additional aerodynamic states in the mathematical model. As mentioned above, in this work the novelty is that although the ROM coefficients to be determined are periodic in time, the procedure proposed for their identification is based on a frequency-domain aerodynamic solution for the perturbed proprotor. In this work, the frequency-domain solution is obtained by applying the Boundary Element Method (BEM) for 3D, unsteady potential flows presented in Ref. [6]. However, the identification procedure proposed is applicable whatever frequency-domain methodology is used for the aerodynamic solution. Details of the procedure followed for the identification of the periodic-coefficient ROM are given in Section 2, for the case of rigid-blade proprotors. The extension to flexible-blade proprotor configurations is examined in Section 3.

A numerical investigation has been performed in order to assess the accuracy of the aerodynamic ROM presented. Specifically, ROM prediction of the aerodynamic loads arising on a three-bladed proprotor connected to a bending and twisting wing has been evaluated for harmonic and damped oscillatory perturbations, and compared with results obtained through direct time-marching aerodynamic solutions.

2. Rigid-blade proprotor

Here, we outline the methodology proposed for the identification of a linear, periodic-coefficient ROM describing the unsteady aerodynamic forces arising on the proprotor blades of a tiltrotor in cruise flight, when perturbed from their helicoidal motion. In this analysis, the complex aerodynamic interaction between proprotor wake and tiltrotor wing is neglected along with transonic and viscous effects, for which a nonlinear model would be necessary for an accurate description. We consider the general problem of an isolated propeller in axial motion in a potential fluid flow, with perturbations that arise from shaft vibrations about its uniform translation cruise motion. In this Section the proprotor blades are assumed to be rigid.

The proposed procedure starts from the observation that, in potential flows, aerodynamic forces are generated by non-zero surface normal components of the body velocity. For the configurations of interest in this work, this is demonstrated in Appendix A through the application of a BEM approach. Indeed, in Appendix A it is shown that a set of N_f generalized aerodynamic blade forces induced by perturbations to a reference steady-state configuration (like, *e.g.,* the cruise axial motion of a proprotor) may be expressed through a frequency-domain relationship of the following type

$$\tilde{\mathbf{f}} = \mathbf{Q}(s)\,\tilde{\boldsymbol{\chi}}, \tag{1}$$

where $\tilde{(\,)}$ denotes Laplace-transformation, and $\mathbf{Q}(s)$ is the $[N_f \times N_c]$ matrix that collects the transfer functions relating the perturbative body-velocity normal components, $\boldsymbol{\chi}$, at the N_c BEM collocation points, to the aerodynamic forces, $\mathbf{f}$.

In order to derive a convenient expression for the body-velocity normal components we observe that, in a frame of reference fixed with the unperturbed flow, a general rigid-body motion of proprotor blades may be expressed by

$$\vec{\mathsf{v}}(\vec{\mathsf{x}},t) = \vec{\mathsf{v}}_{_H}(t) + \vec{\omega}(t) \times (\vec{\mathsf{x}} - \vec{\mathsf{x}}_{_H}), \tag{2}$$

where $\vec{\mathsf{v}}_{_H}$ is the hub velocity, $(\vec{\mathsf{x}} - \vec{\mathsf{x}}_{_H})$ is the distance vector between the hub and an arbitrary blade point $\vec{\mathsf{x}}$, whereas $\vec{\omega}$ is the angular velocity of the blades. Introducing a frame of reference $Hxyz$ rigidly connected to the rotor, centered at the rotor hub and with unit vectors $\vec{\mathsf{i}}_r, \vec{\mathsf{j}}_r, \vec{\mathsf{k}}_r$, the velocity distribution in equation (2) may be expressed through a linear combination of six time-independent vector spacial distributions, $\vec{\Psi}_n$, with coefficients corresponding to the scalar components of $\vec{\mathsf{v}}_{_H}$ and $\vec{\omega}$. Indeed, for

$$\vec{\mathsf{v}}_{_H} = v_{_H}^x\,\vec{\mathsf{i}}_r + v_{_H}^y\,\vec{\mathsf{j}}_r + v_{_H}^z\,\vec{\mathsf{k}}_r,$$

and

$$\vec{\omega} = \omega^x\,\vec{\mathsf{i}}_r + \omega^y\,\vec{\mathsf{j}}_r + \omega^z\,\vec{\mathsf{k}}_r,$$

equation (2) may be recast in the following way

$$\vec{\mathsf{v}}(\vec{\mathsf{x}},t) = \sum_{n=1}^{6} v_n(t)\,\vec{\Psi}_n(\vec{\mathsf{x}}), \tag{3}$$

where the generalized velocity components are defined as

$$v_1 = v_H^x,\ v_2 = v_H^y,\ v_3 = v_H^z,$$
$$v_4 = \omega^x,\ v_5 = \omega^y,\ v_6 = \omega^z,$$

while, for

$$\vec{\mathsf{x}} - \vec{\mathsf{x}}_H = (x - x_H)\,\vec{\mathsf{i}}_r + (y - y_H)\,\vec{\mathsf{j}}_r + (z - z_H)\,\vec{\mathsf{k}}_r,$$

the vector spacial distributions are given by

$$\vec{\Psi}_1(\vec{\mathsf{x}}) = \vec{\mathsf{i}}_r,\ \vec{\Psi}_2(\vec{\mathsf{x}}) = \vec{\mathsf{j}}_r,\ \vec{\Psi}_3(\vec{\mathsf{x}}) = \vec{\mathsf{k}}_r,$$

and,

$$\begin{aligned}
\vec{\Psi}_4(\vec{\mathsf{x}}) &= -(z - z_H)\,\vec{\mathsf{j}}_r + (y - y_H)\,\vec{\mathsf{k}}_r,\\
\vec{\Psi}_5(\vec{\mathsf{x}}) &= (z - z_H)\,\vec{\mathsf{i}}_r - (x - x_H)\,\vec{\mathsf{k}}_r,\\
\vec{\Psi}_6(\vec{\mathsf{x}}) &= -(y - y_H)\,\vec{\mathsf{i}}_r + (x - x_H)\,\vec{\mathsf{j}}_r.
\end{aligned}$$

Next, we note that: (i) through the kynetic relationship between shaft motion and rotor rigid-body motion, for any given perturbation of the shaft motion, it is possible to determine the corresponding generalized rotor velocities, v_n, defined above and, as a consequence, (ii) if the transfer functions relating v_n and forces are known, also forces induced by any shaft perturbation may be determined. Therefore, in equation (1) it is convenient to replace the input column matrix, $\boldsymbol{\chi}$, with its (time-independent) expression given in terms of the rotor generalized velocities, v_n. For χ_m denoting the body-velocity normal component at the collocation point located at $\vec{\mathsf{x}}_m$, we have (see Appendix A)

$$\begin{aligned}
\chi_m(t) &= \vec{\mathsf{v}}(\vec{\mathsf{x}}_m, t) \cdot \vec{\mathsf{n}}(\vec{\mathsf{x}}_m)\\
&= \sum_{n=1}^{6} v_n(t)\,\vec{\Psi}_n(\vec{\mathsf{x}}_m) \cdot \vec{\mathsf{n}}(\vec{\mathsf{x}}_m), \qquad (4)
\end{aligned}$$

where $\vec{\mathsf{n}}(\vec{\mathsf{x}}_m)$ is the unit vector normal to the blade surface at the point $\vec{\mathsf{x}}_m$. Transforming equation (4) into frequency domain and applying this process for the boundary condition at each collocation point yields the following matrix expression

$$\tilde{\boldsymbol{\chi}} = \mathbf{E}^{BC}\,\tilde{\mathbf{v}}, \qquad (5)$$

where $\mathbf{v}$ is the six-element column matrix collecting the generalized velocities, v_n, whereas the entries of the $[N_c \times 6]$ boundary-condition matrix, $\mathbf{E}^{BC}$, are given by

$$E^{BC}_{mn} = \vec{\Psi}_n(\vec{\mathsf{x}}_m) \cdot \vec{\mathsf{n}}(\vec{\mathsf{x}}_m). \qquad (6)$$

Combining equation (1) with equation (5) yields

$$\tilde{\mathbf{f}} = \mathbf{E}(s)\,\tilde{\mathbf{v}}, \qquad (7)$$

where

$$\mathbf{E}(s) = \mathbf{Q}(s)\,\mathbf{E}^{BC}$$

is the $[N_f \times 6]$ aerodynamic transfer-function matrix that relates the generalized rigid-rotor velocities to the corresponding aerodynamic forces. The entries of this matrix are transcendental function of the Laplace variable, s, due to the time-delay terms appearing in the aerodynamic solution from wake-vorticity convection (see Appendix A). An aerodynamic operator of this type would give rise to an infinite-dimension state space problem in the time-domain. Thus, in order to identify the aerodynamic ROM, this difficulty is overcome by utilizing rational expressions for approximating the transfer functions in the aerodynamic matrix. Indeed, through the methodology outlined in Appendix B, it is possible to derive the following approximate rational-matrix expression

$$\mathbf{E}(s) \approx s\,\mathbf{A}_1 + \mathbf{A}_0 + \mathbf{C}\,[s\,\mathbf{I} - \mathbf{A}]^{-1}\,\mathbf{B}, \qquad (8)$$

where $\mathbf{A}_1, \mathbf{A}_0, \mathbf{A}, \mathbf{B}$ and $\mathbf{C}$ are real, fully populated matrices (see also Refs. [7], [8] and [9]). Matrices $\mathbf{A}_1$ and $\mathbf{A}_0$ have dimensions $[N_f \times 6]$, $\mathbf{A}$ is a $[N_a \times N_a]$ matrix containing the N_a poles included in the approximating expression, $\mathbf{C}$ is a $[N_f \times N_a]$ matrix, while $\mathbf{B}$ has dimensions $[N_a \times 6]$. In the expression above, the first-order polynomial truncation is suggested by the fact that the asymptotic behavior of transfer functions between velocities and aerodynamic forces is linear, as induced by the presence of the first time derivative of the velocity potential in the Bernoulli theorem (see matrix $\mathbf{E}_p$ in Appendix A) and by the time-independence of the boundary-condition matrix, $\mathbf{E}^{BC}$.

Next, combining equation (8) with equation (7) and transforming into time domain yields the following constant-coefficient expression relating the generalized rigid-blade velocities (and their first time derivatives) with the corresponding unsteady aerodynamic forces arising on the perturbed blades

$$\begin{aligned}
\mathbf{f}(t) &= \mathbf{A}_1\dot{\mathbf{v}} + \mathbf{A}_0\mathbf{v} + \mathbf{C}\,\mathbf{r} \qquad (9)\\
\dot{\mathbf{r}} &= \mathbf{A}\,\mathbf{r} + \mathbf{B}\,\mathbf{v}, \qquad (10)
\end{aligned}$$

where $\mathbf{r}$ is the column matrix that collects the N_a additional aerodynamic states associated to the poles included in the approximating aerodynamic matrix [a consequence of the flow-memory effects included in matrix $\mathbf{E}(s)$].

The last step in the procedure for the identification of the proprotor aerodynamic ROM is the replacement [in equations (9) and (10)] of the generalized rigid-blade velocities, with the kynetic equations that relate them to the shaft degrees of freedom (or to the gust velocity, if present). Introducing a frame of reference $O_s x_s y_s z_s$ that is rigidly connected with the (nonrotating) shaft, the six degrees of freedom of the perturbative shaft rigid-body motion may be defined by the

small diplacements u_x, u_y, u_z of the origin O_s along the three axes, together with the small rotations $\alpha_x, \alpha_y, \alpha_z$ of the frame about the same axes (note that, for a wing-proprotor system they represent the degrees of freedom of the wing section where the proprotor is attached to). Combining the shaft motion with the helicoidal cruise-state motion defined by the translation velocity $\vec{\mathsf{V}}$ along the unperturbed shaft and the rotational velocity $\vec{\Omega}$ about the same axis, in equation (2) we have

$$\vec{\mathsf{v}}_{_H}(t) = \vec{\mathsf{V}} + \vec{\mathsf{v}}_{_H}^{per} \tag{11}$$

and

$$\vec{\omega}(t) = \vec{\Omega} + \vec{\omega}^{per}, \tag{12}$$

where $\vec{\mathsf{v}}_{_H}^{per} = \vec{\mathsf{v}}_{_H}^{per}(u_x, u_y, u_z, \alpha_x, \alpha_y, \alpha_z)$ and $\vec{\omega}^{per} = \vec{\omega}^{per}(\alpha_x, \alpha_y, \alpha_z)$ denote, respectively, the hub velocity and the rotor angular velocity due to perturbative shaft motion. Then, determining the rotor-frame components of vectors $\vec{\mathsf{v}}_{_H}$ and $\vec{\omega}$, and limiting our analysis to first-order perturbation terms, the following relationship between generalized rigid-blade velocities and shaft degrees of freedom may be determined

$$\mathbf{v}(t) = \mathbf{K}_1(\Omega, t)\,\dot{\mathbf{q}}_{sh} + \mathbf{K}_0(V, \Omega, t)\,\mathbf{q}_{sh}, \tag{13}$$

where $\mathbf{q}_{sh}^T = \{u_x\ u_y\ u_z\ \alpha_x\ \alpha_y\ \alpha_z\}$, whereas $\mathbf{K}_1$ and $\mathbf{K}_0$ are $[6 \times 6]$ time-periodic kynetic matrices (a periodic-coefficient relationship between $\mathbf{v}$ and gust velocity may also be determined for gust-perturbed tiltorotor configurations). Note that the time dependence of the kynetic matrices is due to the relative motion between the rotor frame of reference $Hxyz$ (where the scalar components of the rotor velocity are defined) and the nonrotating shaft frame of reference $O_s x_s y_s z_s$ (where the shaft perturbations are defined). In addition, the dependence of $\mathbf{K}_0$ on V is due to time variation of rotor-frame components of the translation velocity, caused by shaft-frame rotation. In order to explain this, let us assume that the rotor-frame axis, z, and the shaft-frame axis z_s, are both aligned along the shaft, and that initially the rotor axes x and y are parallel to the shaft axes x_s and y_s, respectively. Then, consider the shaft perturbations u_x (translation) and α_x (rotation). We observe that u_x induces a perturbative velocity $\dot{u}_x$ parallel to the x_s shaft axis: in the (rotating) rotor frame it has the following two components

$$v_1 = \dot{u}_x\,\cos(\Omega t), \quad v_2 = -\dot{u}_x\,\sin(\Omega t). \tag{14}$$

In addition, the rotation of the shaft frame yields a $V\,\alpha_x$ perturbation velocity along the shaft y_s axis which, in the of rotor frame, has components

$$v_1 = V\,\alpha_x\,\sin(\Omega t), \quad v_2 = V\,\alpha_x\,\cos(\Omega t). \tag{15}$$

Hence, equation (14) is an example of time-periodic entries of matrix $\mathbf{K}_1$, while examples of time-periodic entries of matrix $\mathbf{K}_0$ depending on the flight velocity V are given in equation (15). Note that the advantage in defining the boundary conditions, $\boldsymbol{\chi}$, in terms of the generalized velocities, $\mathbf{v}$, rather than directly in terms of the shaft degrees of freedom, $\mathbf{q}_{sh}$, is that constant-coefficient relationships are involved. When transformed into frequency domain, they yield the simple transfer function between $\mathbf{v}$ and $\boldsymbol{\chi}$ given in equation (5). On the contrary, equation (13) shows that expressing $\boldsymbol{\chi}$ directly in terms of $\mathbf{q}_{sh}$ would give rise to time periodic-coefficient relationships. In turn, in the frequency domain these would produce complex convolution integral terms, and the rational-matrix approximation would not be applicable to the resulting $\mathbf{E}$, anymore. In that case, the alternative to get a finite-state model could be the application of the rational-matrix approximation to $\mathbf{Q}$ [see equation (1)], with the drawback of requiring the approximation of a number of entries much higher than those appearing in $\mathbf{E}$ (hundreds of collocation points might be introduced by the application of the BEM approach).

Finally, the identification of the proprotor aerodynamic ROM is obtained by combining equations (9) and (10) with equation (13). This yields the following set of equations

$$\begin{aligned} \mathbf{f}(t) &= \mathbf{D}_2(t)\,\ddot{\mathbf{q}}_{sh} + \mathbf{D}_1(t)\,\dot{\mathbf{q}}_{sh} + \mathbf{D}_0(t)\,\mathbf{q}_{sh} + \mathbf{C}\,\mathbf{r} \\ \dot{\mathbf{r}} &= \mathbf{A}\,\mathbf{r} + \mathbf{H}_1(t)\,\dot{\mathbf{q}}_{sh} + \mathbf{H}_0(t)\,\mathbf{q}_{sh}, \end{aligned}$$

where

$$\begin{gathered} \mathbf{D}_2(t) = \mathbf{A}_1\mathbf{K}_1(t), \\ \mathbf{D}_1(t) = \mathbf{A}_1[\dot{\mathbf{K}}_1(t) + \mathbf{K}_0(t)] + \mathbf{A}_0\mathbf{K}_1(t), \\ \mathbf{D}_0(t) = \mathbf{A}_1\dot{\mathbf{K}}_0(t) + \mathbf{A}_0\mathbf{K}_0(t), \\ \mathbf{H}_1(t) = \mathbf{B}\mathbf{K}_1(t), \quad \mathbf{H}_0(t) = \mathbf{B}\mathbf{K}_0(t), \end{gathered}$$

are periodic matrices. For a given time evolution of the shaft perturbative motion variables, $\mathbf{q}_{sh}$, the equations above yield the corresponding aerodynamics forces, $\mathbf{f}$, acting on the blades of the proprotor.

3. Deformable-blade proprotor

In this Section, we extend to deformable-blade configurations the methodology that has been outlined above. In the case of deforming proprotor blades, some additional terms appear in the aerodynamic ROM. These arise from the contribution of blade deflections to the boundary conditions, and imply the inclusion of the degrees of freedom associated to the blade deformation among the perturbation variables.

The effect of blade flexibility on aerodynamic loads is twofold: (i), elastic vibrations yield an additional term, $\vec{\mathsf{v}}_{def}$, in the velocity distribution of equation (2) that becomes

$$\vec{\mathsf{v}}(\vec{\mathsf{x}},t) = \vec{\mathsf{v}}_{_H}(t) + \vec{\omega}(t) \times (\vec{\mathsf{x}} - \vec{\mathsf{x}}_{_H}) + \vec{\mathsf{v}}_{def}(\vec{\mathsf{x}},t) \quad (16)$$

and, (ii), elastic deformation causes rotation of the unit normal vectors, $\vec{\mathsf{n}}$, appearing in the evaluation of the boundary conditions. In order to include these contributions into the aerodynamic ROM, it is convenient to express the elastic deflection, $\vec{\mathsf{d}}_{def}(\vec{\mathsf{x}},t)$, of each rotor blade in terms of the following combination of N_m shape functions

$$\vec{\mathsf{d}}_{def}(\vec{\mathsf{x}},t) = \sum_{l=1}^{N_m} q_l(t)\, \vec{\Phi}_l(\vec{\mathsf{x}}), \quad (17)$$

where the q_l's denote the generalized coordinates of the blade elastic motion, while $\vec{\Phi}_l$ are vector shape functions chosen for the description of the deformation distribution, which have time-independent components in the $Hxyz$ rotor frame. Using equation (17), the blade velocity due to elastic vibration is given by

$$\vec{\mathsf{v}}_{def}(\vec{\mathsf{x}},t) = \sum_{l=1}^{N_m} \dot{q}_l(t)\, \vec{\Phi}_l(\vec{\mathsf{x}}), \quad (18)$$

whereas the unit normals on the deformed-blade surface may be expressed using the following first-order truncation of the Taylor series in terms of the generalized coordinates, *i.e.,*

$$\vec{\mathsf{n}}(\vec{\mathsf{x}},t) = \vec{\mathsf{n}}_{rig}(\vec{\mathsf{x}}) + \sum_{l=1}^{N_m} \frac{\partial \vec{\mathsf{n}}(\vec{\mathsf{x}})}{\partial q_l} q_l(t), \quad (19)$$

where $\vec{\mathsf{n}}_{rig}$ denotes normal vector in the rigid-blade configuration, and $\partial\vec{\mathsf{n}}/\partial q_l$ are vectors with time-constant rotor-frame components [that may be evaluated through equation (17)]. Combining equations (18) and (19) with equation (16), under the assumption of linear analysis, the perturbation boundary conditions at each blade of the proprotor are given by

$$\begin{aligned}
\chi_m(t) &= \vec{\mathsf{v}}(\vec{\mathsf{x}}_m,t) \cdot \vec{\mathsf{n}}(\vec{\mathsf{x}}_m) \\
&= \sum_{n=1}^{6} v_n(t)\, \vec{\Psi}_n(\vec{\mathsf{x}}_m) \cdot \vec{\mathsf{n}}_{rig}(\vec{\mathsf{x}}_m) \\
&+ \sum_{l=1}^{N_m} \dot{q}_l(t)\, \vec{\Phi}_l(\vec{\mathsf{x}}_m) \cdot \vec{\mathsf{n}}_{rig}(\vec{\mathsf{x}}_m) \\
&+ \sum_{l=1}^{N_m} \vec{\mathsf{v}}_{cr} \cdot \frac{\partial \vec{\mathsf{n}}(\vec{\mathsf{x}}_m)}{\partial q_l} q_l(t), \quad (20)
\end{aligned}$$

where $\vec{\mathsf{v}}_{cr} = \vec{\mathsf{V}} + \vec{\Omega} \times (\vec{\mathsf{x}} - \vec{\mathsf{x}}_{_H})$ is the unperturbed proprotor cruise velocity. Transforming equation (20) into frequency domain and repeating this procedure at each control point and for all of the N_b blades of the proprotor, the following matrix expression is obtained

$$\tilde{\boldsymbol{\chi}} = \mathbf{E}^{BC}_{rig}\, \tilde{\mathbf{v}} + \mathbf{E}^{BC}_{def}(s)\, \tilde{\mathbf{q}}_{def}, \quad (21)$$

where $\mathbf{q}_{def}$, is the column matrix collecting the $N_b * N_m$ generalized coordinates, q_l, of the elastic motion of all of the rotor blades, $\mathbf{E}^{BC}_{rig}$ coincides with the matrix defined in equation (6), whereas the entries of the $[N_c \times N_b * N_m]$ matrix $\mathbf{E}^{BC}_{def}$ are given by

$$\begin{aligned}
E^{BC}_{def}(s)_{ml} &= \vec{\mathsf{v}}_{cr}(\vec{\mathsf{x}}_m) \cdot \frac{\partial \vec{\mathsf{n}}(\vec{\mathsf{x}}_m)}{\partial q_l} \\
&+ s\, \vec{\Phi}_l(\vec{\mathsf{x}}_m) \cdot \vec{\mathsf{n}}_{rig}(\vec{\mathsf{x}}_m).
\end{aligned}$$

Introducing the $(6 + N_b * N_m)$-element column matrix

$$\mathbf{w} = \left\{ \begin{array}{c} \mathbf{v} \\ \mathbf{q}_{def} \end{array} \right\}$$

which collects the rotor generalized velocities and blade deformation coordinates, along with the following $[N_c \times (6 + N_b * N_m)]$ boundary-condition matrix

$$\mathbf{E}^{BC}(s) = \left[\begin{array}{cc} \mathbf{E}^{BC}_{rig} & \mathbf{E}^{BC}_{def}(s) \end{array} \right],$$

and combining equation (1) with equation (21) yields

$$\tilde{\mathbf{f}} = \mathbf{E}(s)\, \tilde{\mathbf{w}}, \quad (22)$$

where

$$\mathbf{E}(s) = \mathbf{Q}(s)\, \mathbf{E}^{BC}(s)$$

is the $[N_f \times (6 + N_b * N_m)]$ aerodynamic transfer-function matrix that relates generalized coordinates of blade elastic motion and rigid-body rotor velocities to the corresponding aerodynamic forces.

Akin to the rigid-blade case, in order to determine the aerodynamic finite-state model, this matrix is approximated through a rational-matrix expression. Following Appendix B we may have

$$\mathbf{E}(s) \approx s^2\, \mathbf{A}_2 + s\, \mathbf{A}_1 + \mathbf{A}_0 + \mathbf{C}\, [s\, \mathbf{I} - \mathbf{A}]^{-1}\, \mathbf{B}, \quad (23)$$

where matrices $\mathbf{A}_2, \mathbf{A}_1$ and $\mathbf{A}_0$ have dimensions $[N_f \times (6 + N_b * N_m)]$ and may be conveniently partitioned (see later) in the following way

$$\mathbf{A}_k = \left[\begin{array}{cc} \mathbf{A}^v_k & \mathbf{A}^q_k \end{array} \right]$$

(with $\mathbf{A}^v_2 = \mathbf{0}$). In addition, $\mathbf{A}$ is a square matrix with dimensions $[N_a \times N_a]$, $\mathbf{C}$ is a $[N_f \times N_a]$ matrix, and $\mathbf{B}$ has dimensions $[N_a \times (6 + N_b * N_m)]$ and may be partitioned as

$$\mathbf{B} = \left[\begin{array}{cc} \mathbf{B}^v & \mathbf{B}^q \end{array} \right].$$

With respect to the rigid-blade case, here the $\mathbf{A}_2$-matrix term has been added due to the fact that $\mathbf{E}^{BC}$ is linearly dependent on s, as induced by the presence of the variables associated to the elastic deformation (it is possible to show that the asymptotic behavior of transfer functions between displacements and aerodynamic forces is quadratic, see *e.g.,* Ref. [9]).

Finally, the deformable proprotor aerodynamic ROM is derived by combining equation (23) with equation (22), transforming into time domain and then expressing the generalized rotor rigid-body velocities, $\mathbf{v}$, in terms of the shaft degrees of freedom [equation (13)]. This process yields the following set of equations for the perturbation unsteady aerodynamic forces

$$\mathbf{f}(t) = \mathbf{D}_2(t)\,\ddot{\mathbf{q}} + \mathbf{D}_1(t)\,\dot{\mathbf{q}} + \mathbf{D}_0(t)\,\mathbf{q} + \mathbf{C}\,\mathbf{r} \quad (24)$$

$$\dot{\mathbf{r}} = \mathbf{A}\,\mathbf{r} + \mathbf{H}_1(t)\,\dot{\mathbf{q}} + \mathbf{H}_0(t)\,\mathbf{q}, \quad (25)$$

where the $(6 + N_b * N_m)$-element column matrix of the input variables is defined as

$$\mathbf{q} = \left\{ \begin{array}{c} \mathbf{q}_{sh} \\ \mathbf{q}_{def} \end{array} \right\},$$

and the periodic matrices appearing in equations (24) and (25) are defined through the following partitions

$$\mathbf{D}_j(t) = [\mathbf{D}_j^{sh}(t)\ \mathbf{D}_j^{def}(t)],$$
$$\mathbf{H}_j(t) = [\mathbf{H}_j^{sh}(t)\ \mathbf{H}_j^{def}(t)],$$

with,

$$\mathbf{D}_2^{sh}(t) = \mathbf{A}_1^v \mathbf{K}_1(t),$$
$$\mathbf{D}_2^{def}(t) = \mathbf{A}_2^q,$$
$$\mathbf{D}_1^{sh}(t) = \mathbf{A}_1^v[\dot{\mathbf{K}}_1(t) + \mathbf{K}_0(t)] + \mathbf{A}_0^v \mathbf{K}_1(t),$$
$$\mathbf{D}_1^{def}(t) = \mathbf{A}_1^q,$$
$$\mathbf{D}_0^{sh}(t) = \mathbf{A}_1^v \dot{\mathbf{K}}_0(t) + \mathbf{A}_0^v \mathbf{K}_0(t),$$
$$\mathbf{D}_0^{def}(t) = \mathbf{A}_0^q,$$
$$\mathbf{H}_1^{sh}(t) = \mathbf{B}^v \mathbf{K}_1(t), \quad \mathbf{H}_1^{def}(t) = \mathbf{0},$$
$$\mathbf{H}_0^{sh}(t) = \mathbf{B}^v \mathbf{K}_0(t), \quad \mathbf{H}_0^{def}(t) = \mathbf{B}^q.$$

For a given time evolution of the shaft degrees of freedom, $\mathbf{q}_{sh}$, and of the generalized coordinates of the blade deformation, $\mathbf{q}_{def}$, equations (24) and (25) give the corresponding aerodynamics forces, $\mathbf{f}$, acting on the blades of the proprotor.

4. Numerical results

Now, we present some results of a numerical investigation that has been performed to assess the accuracy the ROM presented above, in predicting the aerodynamic loads arising on a proprotor perturbed from cruise flight conditions. Specifically, we have considered a three-bladed proprotor with radius $R = 3.97$m, and cruise flight defined by axial velocity $V = 25.7$m/s and rotor angular velocity $\Omega = 40.4$rad/s (this corresponds to one of the configurations examined in Ref. [1]). The blade collective-pitch angle varies linearly along the blade span from the root value $\theta_{root} = 33°$, to the tip value $\theta_{tip} = 5°$, whereas the chord length is $c = 0.4778$m. For the results that will be presented in the following, the elastic deformation of the blades has been simulated by a rigid-body flapping motion about a root hinge. Therefore, the proprotor perturbation motion has 9 degrees of freedom, *i.e.,* those related to the shaft motion, $\mathbf{q}_{sh}$, with the addition of one elastic degree of freedom per blade (namely, the flap deflection angle, β).

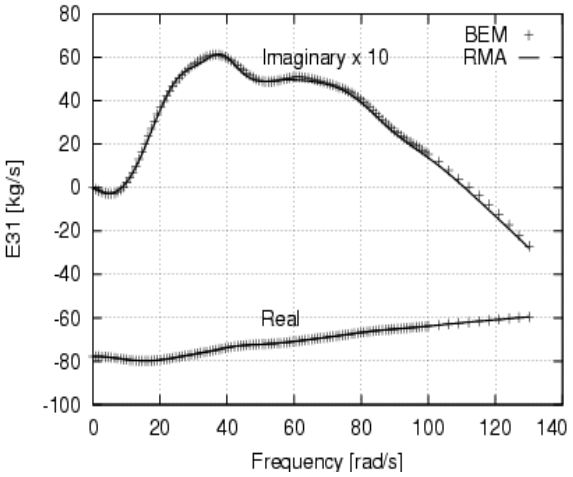

Figure 1. Rational-matrix approximation of transfer function between v_1 and lift force on blade 1.

First, some results concerning the Rational-Matrix Approximation (RMA) of the aerodynamic matrix, $\mathbf{E}(s)$, are shown [see equations (8) and (23)]. For the rotor-fixed frame of reference, $Hxyz$, having the z-axis aligned with the shaft and the y-axis aligned with one of the rotor blades (blade 1), consider the transfer function, $E_{31}(s)$, between the generalized velocity component v_1 (see Section 2) and the lift-force (proprotor thrust) acting on blade 1. Figure 1 shows the comparison between the values of this transfer function computed by the frequency-domain BEM approach outlined in Appendix A, and those given by the rational-matrix approximation, with the introduction of 16 poles. In the frequency range examined, the agreement between the two curves is excellent both for the real part and the imaginary part of the transfer function. The same good accuracy may be observed for all of the transfer functions in matrix $\mathbf{E}$ and, as a further example, we show

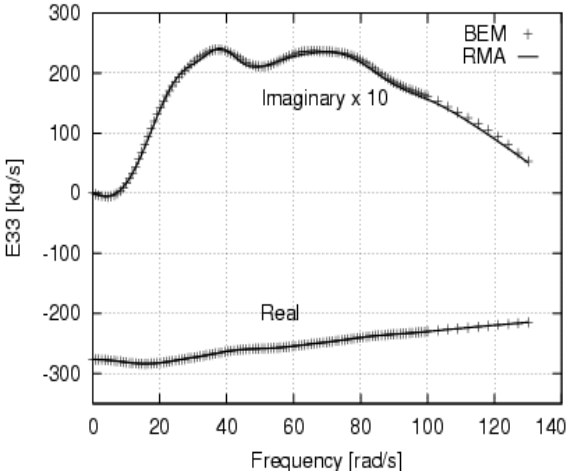

Figure 2. Rational-matrix approximation of transfer function between v_3 and lift force on blade 1.

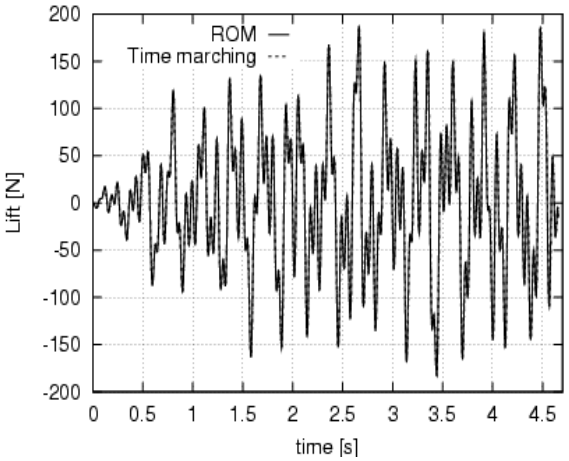

Figure 3. Lift force on blade 1 due to wing/blade harmonic perturbations.

Fig. 2 where computed and approximate values of the transfer function, $E_{33}(s)$, between generalized velocity v_3 and lift-force on blade 1 are compared.

Then, starting from the rational approximation of the aerodynamic transfer functions, following the procedure outlined in Sections 2 and 3, we have determined the aerodynamic ROM of the proprotor considered. In order to assess its accuracy for a realistic case, the proprotor shaft has been assumed to be fixed to the tip section of a tiltrotor wing subject to flapping, w, and torsional, ϑ, elastic motion. Combining this motion with the blade elastic deformations, it is possible to determine the variables to be used as input for the ROM presented in this paper, and thus predict the aerodynamic loads associated to the perturbations considered. In this numerical investigation we have examined two different motions. One is a combination of wing and blade-flapping deformations with an asymptotic harmonic behavior, starting from rest conditions. Specifically, the dynamics of the wing-proprotor is described by the following functions for the time derivative of wing-tip and blade degrees of freedom

$$\begin{aligned}
\dot{w}(t) &= A_w\,(1-e^{-\alpha_w\,t})\sin(\omega_w\,t)\\
\dot{\vartheta}(t) &= A_\vartheta\,(1-e^{-\alpha_\vartheta\,t})\sin(\omega_\vartheta\,t)\\
\dot{\beta}_j(t) &= A_\beta\,(1-e^{-\alpha_\beta\,t})\sin\left[\omega_\beta\,t-(j-1)\frac{2\pi}{3}\right],
\end{aligned}$$

for $j=1,2,3$, with $A_w = 1\text{m/s}$, $A_\vartheta = 0.16\text{rad/s}$, $A_\beta = 0.08\text{rad/s}$, $\omega_w = \Omega/3$, $\omega_\vartheta = 1.5\Omega$, $\omega_\beta = 1.1\Omega$ and $\alpha_w = \alpha_\vartheta = \alpha_\beta = 1\ \text{s}^{-1}$.

The aerodynamic forces associated to this motion have been evaluated both applying the ROM presented in this work and through the time-marching (exact) solution of the time-domain version of the

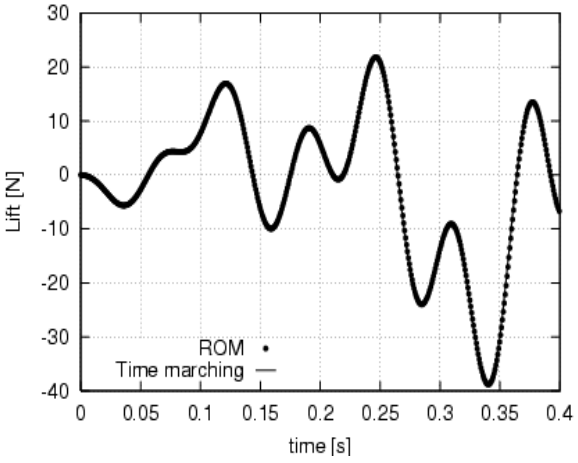

Figure 4. Lift force on blade 1 due to wing/blade harmonic perturbations. Details of the initial evolution.

BEM approach outlined in Appendix A. Figure 3 depicts the lift force acting on blade 1, as computed by both approaches. The two curves cannot be distinguished and the prediction of the reduced-order model is in excellent agreement with the time-marching solution. This is confirmed in Fig. 4 where, changing the scales of the axes, a more detailed analysis of the comparison is shown for the initial part of the motion. The ROM shows the same excellent accuracy in predicting all of the aerodynamic loads examined. As further examples, in Figs. 5 and 6 the comparison between time-marching and ROM predictions is shown for the pitching moment about the mid-chord line and for the moment about the flap hinge on blade 1. Also in these cases, no dif-

ference between the two results can be observed in the figures.

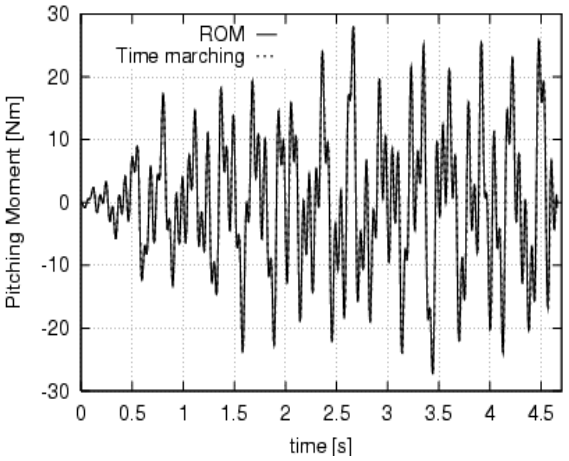

Figure 5. Pitching moment on blade 1 due to wing/blade harmonic perturbations.

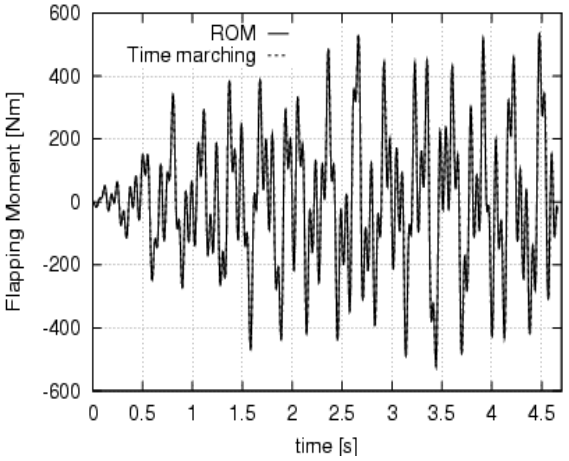

Figure 6. Flapping moment on blade 1 due to wing/blade harmonic perturbations.

The second wing-proprotor perturbation motion that has been examined simulates the damped oscillations of a stable wing perturbed from an equilibrium configuration (the rotor blades are assumed to be rigid). Specifically, the wing motion considered is given by the following expressions

$$w(t) = A_w\, e^{-\alpha_w\, t}\, \sin(\omega_w\, t)$$
$$\vartheta(t) = A_\vartheta\, e^{-\alpha_\vartheta\, t}\, \sin(\omega_\vartheta\, t),$$

with $A_w = R/5$, $A_\vartheta = \pi/20$, $\alpha_w = 0.2\text{s}^{-1}$, $\alpha_\vartheta = 0.4\text{s}^{-1}$, whereas the values of ω_w and ω_ϑ are equal to those used in the analysis discussed above.

Lift force, pitching moment and flapping moment on blade 1 due to these perturbations are depicted

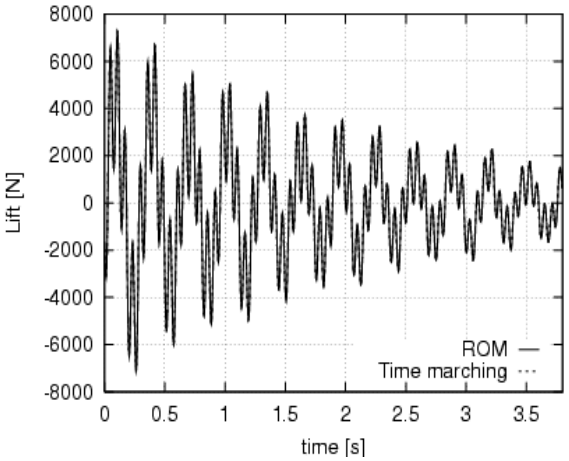

Figure 7. Lift force on blade 1 due to wing/blade damped perturbations.

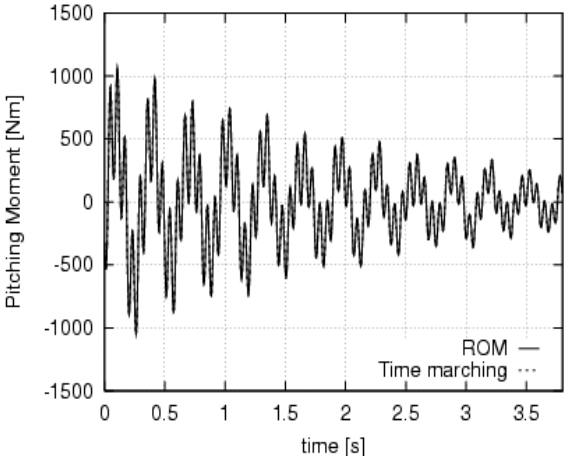

Figure 8. Pitching moment on blade 1 due to wing/blade damped perturbations.

in Figs. 7, 8 and 9, respectively, both as predicted by the ROM approach and as computed through the BEM time-marching solution. Akin to the harmonic input case, also for the damped motion the solution predicted by the ROM approach is very accurate. Taking the flapping moment as an example, Figs. 10 and 11 demonstrate that the same high level of accuracy is obtained for the loads on the other two rotor blades, as well.

Finally, we have examined the sensitivity of the ROM presented on the accuracy of the rational-matrix approximation. In particular, we have analyzed the effect of decreasing the number of additional aerodynamic states (for the sake of simplicity of the aeroelastic model and reduction of computational costs, it is desirable to have as few

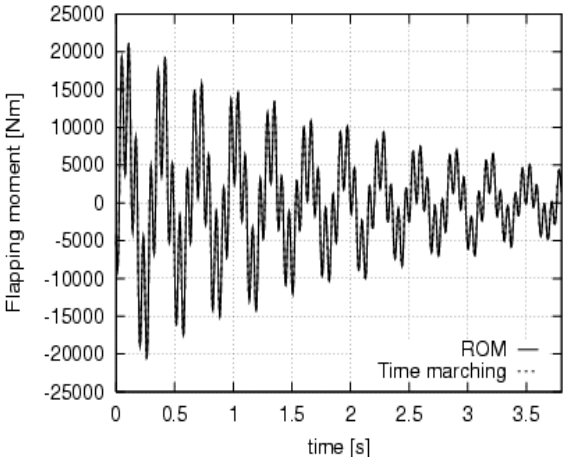

Figure 9. Flapping moment on blade 1 due to wing/blade damped perturbations.

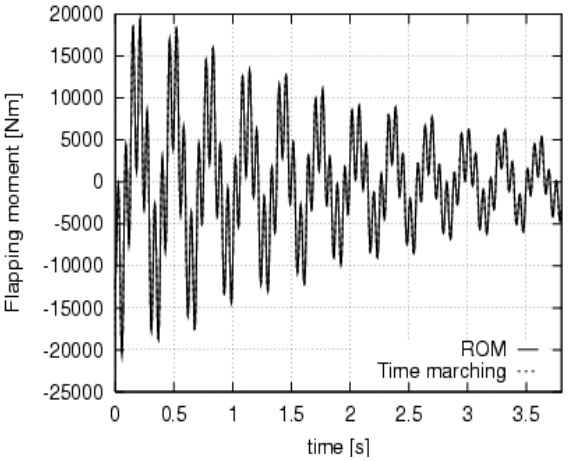

Figure 11. Flapping moment on blade 3 due to wing/blade damped perturbations.

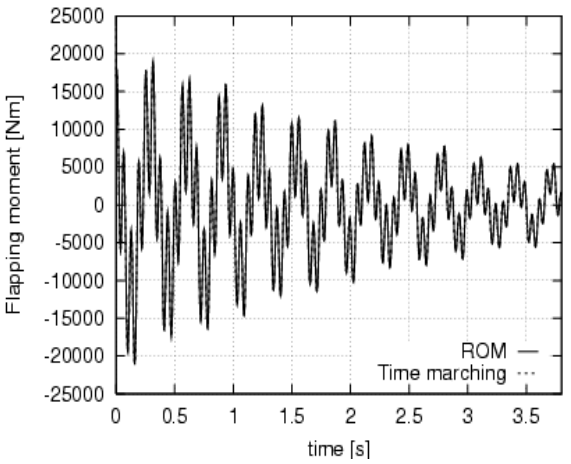

Figure 10. Flapping moment on blade 2 due to wing/blade damped perturbations.

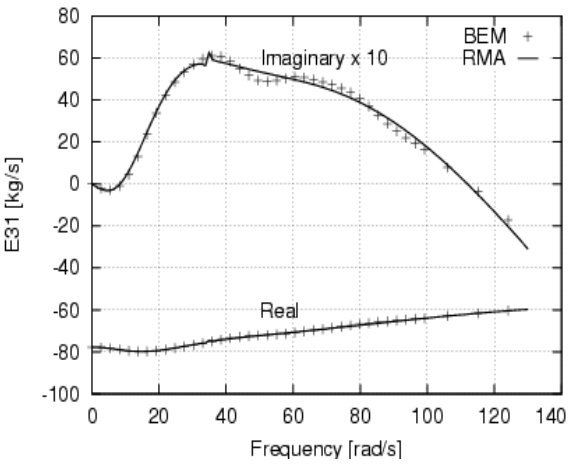

Figure 12. Rational-matrix approximation of transfer function between v_1 and lift force on blade 1, using 8 poles.

additional aerodynamic states as possible). Figure 12 shows the rational approximation of the transfer function between the velocity component v_1 and the lift force on blade 1 obtained using 8 poles (*i.e.,* half of those used for the results in Fig. 1). The agreement with the values computed through the frequency-domain BEM approach is satisfactory, but it is not so good as that of Fig. 1. However, it is interesting to observe that, despite the reduction of the aerodynamic states, the accuracy of the predictions given by the resulting aerodynamic ROM remains excellent. This is shown in Fig. 13 for the lift force on blade 1 induced by harmonic perturbations.

Concluding remarks

A periodic-coefficient ROM for the prediction of unsteady aerodynamic loads arising on tiltrotor propellers perturbed from horizontal cruise flight conditions has been presented. Despite the time dependence of the model coefficients, it is determined through the application of a frequency-domain aerodynamic solver, followed by a rational approximation of the resulting transfer functions between kynetic degrees of freedom and aerodynamic loads. Due to this rational approximation, the ROM description requires the inclusion of some aerodynamic states to be added to the kynetic degrees of freedom. In this paper, the frequency-domain aerodynamic solution has been

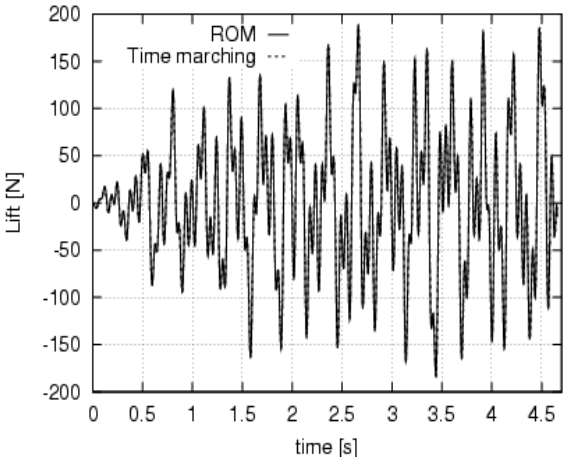

Figure 13. Lift force on blade 1 due to wing/blade harmonic perturbations. ROM from a 8-pole rational-matrix approximation.

obtained by a BEM approach. However, the procedure described for determining the ROM is general and applicable whatever frequency-domain solution is available.

In the numerical investigation for the assessment of ROM accuracy, a three-bladed proprotor with flapping blades and shaft fixed to the tip section of a flapping and twisting wing has been examined. Aerodynamic loads arising both from harmonic and damped oscillatory perturbations of the wing-proprotor system have been calculated. Using the results from a time-marching (exact) BEM solution as comparison, the ROM presented here has demonstrated to be capable to predict with excellent accuracy the loads induced by both types of perturbations. In addition, the numerical investigation has also shown that the accuracy of the aerodynamic ROM remains excellent if the rational approximation of the aerodynamic transfer functions is based on a number of poles reduced with respect to those of the optimal solution. This implies that simplified versions of this aerodynamic ROM give reliable predictions, and this is extremely useful from the preliminary-design and control-synthesis points of view.

References

1. Johnson, W., "Dynamics of Tilting Proprotor Aircraft in Cruise Flight," NASA TN D-7677, May 1974.
2. Nixon, M.W., "Aeroelastic response and Stability of Tiltrotors with Elastically-Coupled Composite Rotor Blades," Ph.D. Thesis, University of Meryland, 1993.
3. Srinivas, V. and Chopra, I., "An Assessment of Aeroelastic Analyses for Tiltrotor Aircraft," 37th AIAA/ASME/ASCE/-AHS/ASC Structures, Structural Dynamics and Materials Conference and Adaptive Structures Forum, Salt Lake City, Utah, April 1996.
4. Nixon, M.W., Piatak, D.J., Corso, L.M. and Popelka, D.A., "Aeroelastic Tailoring for Stability Augmentation and Performance Enhancements of Tiltrotor Aircraft," CEAS/AIAA/ICASE/NASA LaRC International Forum on Aeroelasticity and Structural Dynamics, Williamsburg, VA, June 1999.
5. Stettner, M., Schrage, D.P. and Peters, D.A., "Application of a State-Space Wake Model to Tiltrotor Wing Unsteady Aerodynamics," American Helicopter Society Aeromechanics Specialists Conference, San Francisco, California, January 1994.
6. Morino, L. and Gennaretti, M., "Boundary Integral Equation Methods for Aerodynamics," in: S.N. Atluri (Ed.), Computational Nonlinear Mechanics in Aerospace Engineering, *Aeronautics & Astronautics AIAA Series*, Vol. 146, 1992.
7. Morino, L., Mastroddi, F., De Troia, R., Ghiringhelli, G.L. and Mantegazza, P. "Matrix fraction approach for finite-state aerodynamic modeling," *AIAA Journal* Vol. 33, pp. 703-711, 1995.
8. Gennaretti, M. and Lisandrin, P., "Flap-Lag Rotor Dynamics and Aeroelastic Stability Using Finite-State Aerodynamics," 24th European Rotorcraft Forum, Marseilles, France, Sept., 1998.
9. Gennaretti, M. and Iemma, U., "Aeroacoustoelasticity in state-space format using CHIEF regularization," *Journal of Fluids and Structures* Vol. 17, No. 7, pp. 983-999, 2003.
10. Morino, L., "A General Theory of Unsteady, Compressible, Potential Aerodynamics," NASA CR-2464, 1974.

Appendix A. BEM formulation for frequency-domain potential aerodynamics

Consider a body moving in an inviscid fluid. If initially the flow is irrotational, it remains irrotational at all times, except for the points which come in contact with the body surface, $\mathcal{S}_B$, since for these points Kelvin's theorem is no longer applicable (see, *e.g.,* Ref. [6]). These points form a surface, $\mathcal{S}_W$ (the wake), where vorticity may be different from zero.

For $\vec{\mathrm{v}}_f$ denoting the velocity of the fluid particles, it is possible to introduce the potential function ϕ such that $\vec{\mathrm{v}}_f = \nabla\phi$ (for $\vec{\mathrm{x}}$ outside $\mathcal{S}_B \cup \mathcal{S}_W$). Assuming the flow incompressible, combining the above equation with the continuity equation, $\nabla\cdot\vec{\mathrm{v}}_f = 0$, one obtains the following Laplace equation

$$\nabla^2\phi = 0 \qquad \text{for } \vec{\mathrm{x}} \text{ outside } \mathcal{S}_B \cup \mathcal{S}_W .$$

This differential equation requires the definition of boundary conditions both over the body and over the wake. The first one is determined from the assumption of body surface impermeability. Accordingly, on $\mathcal{S}_B$ we have $(\vec{\mathrm{v}}_f - \vec{\mathrm{v}}_B)\cdot\vec{\mathrm{n}} = 0$, where $\vec{\mathrm{v}}_B$ is the velocity of the body-surface points and $\vec{\mathrm{n}}$ is its outward unit normal. Recalling that $\vec{\mathrm{v}}_f = \nabla\phi$, the body boundary condition reads

$$\frac{\partial\phi}{\partial n} = \vec{\mathrm{v}}_B \cdot \vec{\mathrm{n}}.$$

The boundary conditions on the wake are obtained from the principles of conservation of mass and momentum across a surface of discontinuity. Recalling the results presented in Ref. [6], these are expressed as: (*i*) $\Delta(\partial\phi/\partial n) = 0$ on $\mathcal{S}_W$, and (*ii*) $\Delta\phi$ =const. following a wake material point (with Δ denoting jump across the wake).

Starting from this differential formulation and applying the boundary integral equation technique, for lifting body configurations with the wake surface fixed with respect to a body-fixed frame of reference (as it occurs, for instance, in translating wings, hovering rotors and propellers in axial motion), it possible to derive the following frequency-domain, incompressible-flow potential solution for $\vec{\mathrm{x}}_* \in \mathcal{S}_B$ (see Refs. [6] and [10] for further details)

$$\begin{aligned}\frac{1}{2}\tilde{\phi}(\vec{\mathrm{x}}_*) &= \int_{\mathcal{S}_B}\left(\frac{\partial\tilde{\phi}}{\partial n}\,G - \tilde{\phi}\,\frac{\partial G}{\partial n}\right)\mathrm{d}\mathcal{S}(\vec{\mathrm{x}}) \\ &\quad - \int_{\mathcal{S}_W}\Delta\tilde{\phi}^{TE}\exp(-s\,\tau)\,\frac{\partial G}{\partial n}\,\mathrm{d}\mathcal{S}(\vec{\mathrm{x}}). \qquad (26)\end{aligned}$$

In equation (26), $G = -1/4\pi\|\vec{\mathrm{x}} - \vec{\mathrm{x}}_*\|$ is the unit source solution of the Laplace equation, whereas τ is the time necessary to convect the material wake point from the trailing edge to the current position. Note that, for configurations where the wake surface is not fixed with respect to the body-fixed frame of reference the frequency-domain integral equation (26) would not be achievable, in that frequency convolution integrals would appear in the description of wake contribution.

Numerical solution of equation (26) can be evaluated from its algebraic approximation. It is derived discretizing the body surface into N_B quadrilateral panels and the wake surface into N_W quadrilateral panels. Assuming ϕ, $\partial\phi/\partial n$ and $\Delta\phi$ constant over each panel [*i.e.,* using a zeroth-order Boundary-Element Method (BEM)], and satisfying equation (26) at the $N_c = N_B$ centers of the panels (collocation points) yields the following algebraic approximation (see Ref. [10] for details)

$$\begin{aligned}\frac{1}{2}\tilde{\phi}_k &= \sum_{j=1}^{N_B} B_{kj}\,\tilde{\chi}_j + \sum_{j=1}^{N_B} C_{kj}\,\tilde{\phi}_j \\ &\quad + \sum_{n=1}^{N_W} F_{kn}\,\Delta\tilde{\phi}_n^{TE}, \qquad (27)\end{aligned}$$

with

$$\chi_j = \left.\frac{\partial\phi}{\partial n}\right|_{\vec{\mathrm{x}}=\vec{\mathrm{x}}_j}, \quad \phi_j = \phi(\vec{\mathrm{x}}_j)$$

and

$$\Delta\phi_n^{TE} = \Delta\phi(\vec{\mathrm{x}}_n^{TE}),$$

where $\vec{\mathrm{x}}_j$ is the j-th collocation point and $\vec{\mathrm{x}}_n^{TE}$ is the trailing edge point from which the wake point at the center of the n-th wake panel was emanated. The coefficients appearing in equation (27) are given by

$$B_{kj} = \int_{\mathcal{S}_{B_j}} G_k\,\mathrm{d}\mathcal{S}, \quad C_{kj} = -\int_{\mathcal{S}_{B_j}}\frac{\partial G_k}{\partial n}\,\mathrm{d}\mathcal{S},$$

$$F_{kn} = -\exp(-s\tau_n)\int_{\mathcal{S}_{W_n}}\frac{\partial G_k}{\partial n}\,\mathrm{d}\mathcal{S},$$

where $G_k = G|_{\vec{\mathrm{x}}_*=\vec{\mathrm{x}}_k}$, and $\mathcal{S}_{Bj}$ and $\mathcal{S}_{Wn}$ denote the surfaces of the j-th panel of $\mathcal{S}_B$ and of the n-th panel of $\mathcal{S}_W$, respectively.

Finally, expressing the potential discontinuity, $\Delta\phi_n^{TE}$, in terms of the values of potential at the center of the corresponding body trailing-edge panel through the relation

$$\Delta\tilde{\phi}_n^{TE} = \sum_{j=1}^{N_B} S_{nj}\,\phi_j,$$

where $S_{nj} = 1(-1)$ if the j-th element is the upper(lower)-surface element located at the trailing edge position from which the n-th wake element was emanated, and $S_{nj} = 0$ otherwise,

equation (27) may be recast in the following matrix form,

$$\tilde{\boldsymbol{\phi}} = \mathbf{E}_\phi(s)\,\tilde{\boldsymbol{\chi}}. \tag{28}$$

In the above equation, $\boldsymbol{\phi}$ is the column matrix collecting the ϕ_j's, $\boldsymbol{\chi}$ is the column matrix collecting the χ_j's and $\mathbf{E}_\phi$ is a $[N_c \times N_c]$ matrix given by

$$\mathbf{E}_\phi(s) = \left[\frac{1}{2}\mathbf{I} - \mathbf{C} - \mathbf{F}(s)\,\mathbf{S}\right]^{-1}\mathbf{B}. \tag{29}$$

Generalized aerodynamic forces

Once the potential distribution over the lifting body has been evaluated, the application of the Bernoulli theorem yields the pressure distribution and, through integration, the generalized aerodynamic forces.

In a frame of reference connected with the body, the Bernoulli theorem has the form

$$\frac{\partial\phi}{\partial t} - \vec{\mathrm{v}}_{_B}\cdot\nabla\phi + \frac{\|\vec{\mathrm{v}}_f\|^2}{2} + \frac{p}{\rho} = \frac{p_\infty}{\rho}, \tag{30}$$

where p denotes local pressure, p_∞ is the pressure of the undisturbed flow, ρ denotes air density, and $\partial/\partial t$ denotes time derivative in a blade-fixed frame. Letting $\phi_{_0}$ and $p_{_0}$ denote, respectively, the velocity potential and the corresponding pressure field around the body in its reference configuration (reference aerodynamic solution), and φ and p' denote, respectively, velocity potential and pressure field produced by perturbation motion, then one has $\phi = \phi_{_0} + \varphi$ and $p = p_{_0} + p'$. Substituting these expressions in equation (30), dropping reference-state and second-order perturbative terms, and transforming into frequency-domain yields the following linearized expression for the pressure perturbation

$$\tilde{p'} = -\rho\,[s\tilde{\varphi} + (\nabla\phi_{_0} - \vec{\mathrm{v}}_{_B})\cdot\nabla\tilde{\varphi}]. \tag{31}$$

Using the body panel-discretization introduced above, and expressing $\nabla\tilde{\varphi}$ through the potential evaluated at the blade collocation points, equation (31) may be recast in the following matrix form

$$\tilde{\mathbf{p}}' = \mathbf{E}_p(s)\,\tilde{\boldsymbol{\varphi}}, \tag{32}$$

where $\mathbf{p}'$ and $\boldsymbol{\varphi}$ are column matrices that collect the values of the perturbation pressure and of the perturbation potential at the collocation points, respectively.

Then, the generalized perturbation forces are defined through the following expression

$$f_n = -\int_{\mathcal{S}_{_B}} p'\,\vec{\mathrm{n}}\cdot\vec{\Upsilon}_n(\vec{\mathrm{x}})\,\mathrm{d}\mathcal{S}(\vec{\mathrm{x}}),$$

where $\vec{\Upsilon}_n$ are a set of N_f vector shape functions with time-constant components in a frame of reference connected with the undeformed body. Note that for aeroelastic analysis, this set of shape functions has to coincide with that used for defining the body rigid and elastic motion [*i.e.,* with the shape functions appearing in equations (3) and (17), in our case]. Then, considering again the body surface discretization applied in the BEM formulation, the following matrix relationship may be obtained in the frequency domain

$$\tilde{\mathbf{f}} = \mathbf{E}_f\,\tilde{\mathbf{p}}', \tag{33}$$

where the entries of the $[N_f \times N_c]$ matrix $\mathbf{E}_f$ are defined as

$$E_{f_{nj}} = -\int_{\mathcal{S}_{_{Bj}}} \vec{\mathrm{n}}\cdot\vec{\Upsilon}_n(\vec{\mathrm{x}})\,\mathrm{d}\mathcal{S}(\vec{\mathrm{x}}),$$

with $\mathcal{S}_{_{Bj}}$ denoting the surface of the j-th body panel.

Finally, combining equation (28) (written for perturbative variables) with equations (32) and (33) yields the following linear relationship between boundary conditions and generalized aerodynamic forces associated to a small-perturbation motion of the body

$$\tilde{\mathbf{f}} = \mathbf{Q}(s)\,\tilde{\boldsymbol{\chi}}, \tag{34}$$

where the $[N_f \times N_c]$ matrix $\mathbf{Q}$ is given by

$$\mathbf{Q}(s) = \mathbf{E}_f\,\mathbf{E}_p(s)\,\mathbf{E}_\phi(s). \tag{35}$$

Appendix B. Matrix-fraction approximation

Here, a procedure for the matrix-fraction approximation of the aerodynamic matrix is briefly outlined. Observing that the frequency asymptotic behavior of aerodynamic transfer functions is quadratic if the inputs are degrees of freedom representing displacements, whereas it is linear if the inputs represent velocity components, the formulation introduced in Ref. [7] suggests the following general matrix-fraction approximation for an aerodynamic matrix

$$\mathbf{E}(s) \approx \hat{\mathbf{E}}(s) = s^2\,\hat{\mathbf{A}}_2 + s\,\hat{\mathbf{A}}_1 + \hat{\mathbf{A}}_0 + \left[\sum_{i=0}^{N}\mathbf{D}_i s^i\right]^{-1}\left[\sum_{i=0}^{N-1}\mathbf{R}_i s^i\right] \tag{36}$$

(with $\hat{\mathbf{A}}_2 = \mathbf{0}$ for velocity-component inputs). Matrices $\hat{\mathbf{A}}_i, \mathbf{D}_i$ and $\mathbf{R}_i$ are real and fully populated (except for $\mathbf{D}_N$ that is chosen to be an

identity matrix). They are determined by a least-square approximation technique along the imaginary axis. Specifically, the satisfaction of the following condition is required

$$\epsilon^2 = \sum_n w_n \,\mathsf{Tr}\left[\mathbf{Z}^*(s_n)\,\mathbf{Z}(s_n)\right]\Big|_{s_n=i\omega_n} = \min,$$

where $i = \sqrt{-1}$, w_n denotes a suitable set of weights, and

$$\mathbf{Z}(s) := \left[\sum_{n=0}^{N} \mathbf{D}_n s^n\right]\left[s^2\,\hat{\mathbf{A}}_2 + s\,\hat{\mathbf{A}}_1 + \hat{\mathbf{A}}_0 - \mathbf{E}(s)\right] + \sum_{n=0}^{N-1} \mathbf{R}_n s^n$$

is a measure of the error $(\mathbf{E} - \hat{\mathbf{E}})$.

Next, in order to use the matrix-fraction approximation for deriving an aerodynamic ROM in state-space format, it is convenient to recast equation (36) in the following form

$$\hat{\mathbf{E}}(s) = s^2\hat{\mathbf{A}}_2 + s\hat{\mathbf{A}}_1 + \hat{\mathbf{A}}_0 + \hat{\mathbf{C}}\left[s\mathbf{I} - \hat{\mathbf{A}}\right]^{-1}\hat{\mathbf{B}}, \quad (37)$$

where $\hat{\mathbf{B}}$ depends upon the $\mathbf{R}_i$'s, $\hat{\mathbf{A}}$ upon the $\mathbf{D}_i$'s, whereas $\hat{\mathbf{C}}^T = [\mathbf{I}, \mathbf{0}, ..., \mathbf{0}]$ (see Ref. [7] or Ref. [9], for details). The accuracy of the approximation depends upon the number, N, of matrices used in the matrix-fraction term in equation (36). The appropriate value of N depends upon the characteristics and number of functions to be approximated. The number of poles included in the approximate expression is linearly related to the value of N. If a high number of poles is introduced, some of them could be found to be unstable, *i.e.,* they could have real part greater than zero: these are spurious poles which are introduced by the interpolation procedure, and are not physically acceptable (if the input kynetic variables have limited amplitudes, aerodynamic forces have limited amplitudes, as well). In order to overcome this problem, the iterative procedure suggested in Ref. [7] is adopted. This consists of: (*i*) diagonalization (or block-diagonalization) of $\hat{\mathbf{A}}$, (*ii*) truncation of the unstable poles (the matrix $\hat{\mathbf{A}}$ is modified into a smaller matrix $\mathbf{A}$), and (*iii*) application of an optimal fit iterative procedure to determine new matrices $\mathbf{A}_2, \mathbf{A}_1, \mathbf{A}_0, \mathbf{C}$, and $\mathbf{B}$ that replace, respectively, $\hat{\mathbf{A}}_2, \hat{\mathbf{A}}_1, \hat{\mathbf{A}}_0, \hat{\mathbf{C}}$, and $\hat{\mathbf{B}}$ (whereas $\mathbf{A}$ remains unchanged throughout the iteration). Hence, the matrix-fraction approximation assuring a good and stable fit of $\mathbf{E}(s)$ has the final form

$$\mathbf{E}(s) \approx s^2\,\mathbf{A}_2 + s\,\mathbf{A}_1 + \mathbf{A}_0 + \mathbf{C}\left[s\,\mathbf{I} - \mathbf{A}\right]^{-1}\mathbf{B}.$$